Injectable preformed scaffolds with shape-memory properties

Sidi A. Bencherif[a,b], R. Warren Sands[a], Deen Bhatta[a], Praveen Arany[a,b], Catia S. Verbeke[a], David A. Edwards[a,b], and David J. Mooney[a,b,1]

[a]School of Engineering and Applied Sciences, Harvard University, Cambridge, MA 02138; and [b]Wyss Institute for Biologically Inspired Engineering at Harvard University, Boston, MA 02115

Edited by David A. Tirrell, California Institute of Technology, Pasadena, CA, and approved October 16, 2012 (received for review July 6, 2012)

Injectable biomaterials are increasingly being explored to minimize risks and complications associated with surgical implantation. We describe a strategy for delivery via conventional needle–syringe injection of large preformed macroporous scaffolds with well-defined properties. Injectable 3D scaffolds, in the form of elastic sponge-like matrices, were prepared by environmentally friendly cryotropic gelation of a naturally sourced polymer. Cryogels with shape-memory properties may be molded to a variety of shapes and sizes, and may be optionally loaded with therapeutic agents or cells. These scaffolds have the capability to withstand reversible deformations at over 90% strain level, and a rapid volumetric recovery allows the structurally defined scaffolds to be injected through a small-bore needle with nearly complete geometric restoration once delivered. These gels demonstrated long-term release of biomolecules in vivo. Furthermore, cryogels impregnated with bioluminescent reporter cells provided enhanced survival, higher local retention, and extended engraftment of transplanted cells at the injection site compared with a standard injection technique. These injectable scaffolds show great promise for various biomedical applications, including cell therapies.

syringe-injectable hydrogels | cryogelation | shape retention | controlled delivery | cell therapy

Hydrogels are 3D networks that can absorb a large amount of water while maintaining their structural integrity. They are considered as appropriate scaffolds for tissue engineering applications mainly due to their structural similarities with native soft tissue, and are widely used as soft materials in many biomedical applications including cell culture, cell encapsulation, controlled delivery of therapeutic agents, and medical device fabrication (1–6).

Hydrogels typically exhibit a nanoporous network structure, but it is advantageous to use hydrophilic networks with large interconnected pores (>10 μm) to allow cell infiltration and deployment, and provide an increased surface area for cell attachment and interaction. As a result, macroporous hydrogel scaffolds have been developed using various techniques such as fiber bonding, gas foaming, microemulsion formation, phase separation, freeze-drying, and porogen leaching (7–15). More recently, gelation at subzero temperatures, known as cryogelation, has been used to create hydrogels with large interconnected pores (16–18). During cryogelation, the reactants are restricted to the unfrozen/semifrozen phases and form a cross-linked network upon polymerization, while the ice crystals nucleated from the aqueous phase during freezing function as porogens. The melting of these ice crystals at temperature above the freezing temperature gives rise to interconnected macroporous networks. Cryogels typically exhibit enhanced mechanical stability with respect to traditional hydrogels (17). Recent studies have shown the potential application of cryogels as tissue engineering scaffolds (19-21).

Due to the trauma resulting from surgical implantation of 3D scaffolds, minimally invasive surgical approaches to deliver polymeric scaffolds have been the focus of recent work (22, 23). For a biomaterial to be injectable, it has to be able to flow through a small-bore needle or a catheter. Most injectable hydrogels are delivered in the liquid form (24–26). However, injecting a liquid that will subsequently polymerize in situ presents a number of complicating issues, including appropriate gelling time, the need to maintain proper gelation conditions, formation of gels with appropriate mechanical strength and persistence time, biocompatibility, and the ability to protect the cargo of protein drugs or cells in adverse environments (27). Finally, purely liquid precursor solutions may leak into the neighboring tissue or dilute with body fluids, which may not only limit hydrogel formation but also limit control over the macrostructure of the gel. Recently, hydrogels with shear-thinning behaviors have been developed to address certain of these concerns (27, 28), but these still do not allow one to precisely control gel location nor create defined macrostructures. Unlike most in situ gelling systems, injectable cryogels have an interconnected macroporous architecture, which appears advantageous over nanoporous hydrogel scaffolds with respect to their ability to facilitate cellular infiltration and trafficking.

We investigate here the potential of a fully preformed cryogel to be delivered into the body through a conventional needle–syringe injection. Alginate, a naturally occurring polysaccharide, which consists of residues of α-L-guluronic and β-D-mannuronic acid, was used to fabricate the scaffolds, as it is considered to be biocompatible (29). Several material properties were investigated to benchmark these cryogels as an injectable scaffold. Key requirements include the following: (*i*) the injectable scaffold must be compressible and flow under moderate pressure; (*ii*) the cryogel should maintain sufficient integrity and strength during injection for gel recovery; (*iii*) once delivered, the cryogel should rapidly regain its original shape and size from the collapsed state; and finally (*iv*) the scaffold should retain biomolecules/cells within the scaffold during the injection process and allow their subsequent release in vivo in a controlled fashion.

Results

Macroporous Hydrogel Synthesis. To prepare alginate amenable to cryogelation, pendant methacryloyl groups were first introduced into the alginate main chains (Fig. 1*A*). ^{1}H NMR spectrum of methacrylated (MA)-alginate exhibited peaks of vinyl methylene and methyl protons at δ5.8 and 5.3, and 1.7, respectively, that were newly formed by the reaction of polymer with 2-aminoethyl methacrylate (AEMA) (Fig. S1). The methacrylation efficiency was calculated based on the ratio of the integrals for alginate protons to the methylene protons of methacryloyl groups, and MA-alginate macromonomer was found to have an approximate degree of methacrylation of 50%.

Next, alginate hydrogels were prepared both at room temperature (RT) and subzero temperature, which were designated as conventional nanoporous hydrogels and macroporous cryogels, respectively. Macroporous 3D alginate cryogels were prepared using MA-alginate by the process of cryogelation at −20 °C using

Author contributions: S.A.B., R.W.S., D.A.E., and D.J.M. designed research; S.A.B., R.W.S., D.B., P.A., and C.S.V. performed research; S.A.B., R.W.S., and D.J.M. analyzed data; and S.A.B. and D.J.M. wrote the paper.

The authors declare no conflict of interest.

This article is a PNAS Direct Submission.

[1]To whom correspondence should be addressed. E-mail: mooneyd@seas.harvard.edu.

This article contains supporting information online at www.pnas.org/lookup/suppl/doi:10.1073/pnas.1211516109/-/DCSupplemental.

www.pnas.org/cgi/doi/10.1073/pnas.1211516109

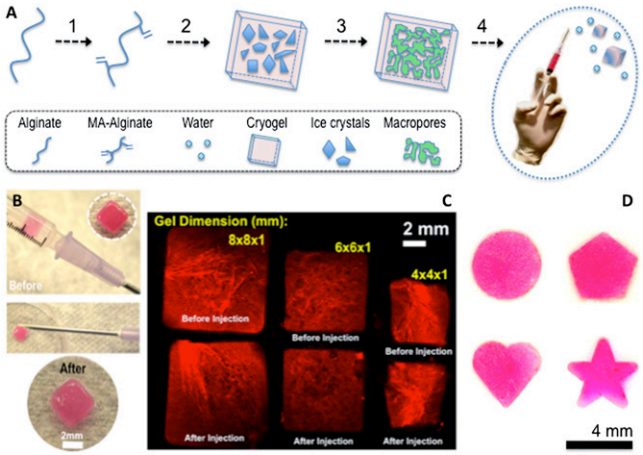

Fig. 1. (*A*) Overview of the cryogelation process: alginate is chemically modified to allow radical polymerization (1); MA-alginate is added to APS/TEMED initiator system before incubation at −20 °C to allow ice crystal formation (2); the process of cryogelation takes place via the following steps: phase separation with ice crystal formation, cross-linking, and polymerization followed by thawing of ice crystals (porogens) to form an interconnected porous cryogel network (3); and conventional needle–syringe injection of preformed cryogels (4). (*B*) Photographs showing placement of a cryogel in 1-mL syringe (before injection) and gel recovery (after injection) via a conventional 16-gauge needle. (*C*) Rhodamine-labeled 1% MA-alginate gels with various sizes and shapes can be easily prepared by cryogenic polymerization. Fluorescent square-shaped gels suspended in 0.2 mL of PBS were syringe injected with a complete geometric restoration as illustrated in the microscopy image before/after injection. (*D*) Photographs showing cryogels prepared with different geometric shapes (disk, pentagon, heart, and star) retained their original shapes after syringe injection.

a free-radical cross-linking mechanism. During cryotropic gelation, most of the solvent (water) is frozen, and the dissolved solutes (macromonomers and initiator system) are concentrated in small semifrozen regions called nonfrozen liquid microphase, in which the free-radical cryopolymerization and gelation proceeds with time (Fig. 1*A*). After complete polymerization, and when subsequently incubated at RT and washed with water to remove unreacted polymeric precursors, the ice crystals melt and leave behind a system of large, continuously interconnected pores. A unique feature of these cryogels is that when an appropriate mechanical force is applied, the gel will shear-collapse, resulting in a biomaterial that flows through a conventional-gauge needle (Fig. 1 *A* and *B*). Unlike traditional nanoporous alginate hydrogels, which are rather brittle, MA-alginate cryogels are elastic, soft, sponge-like materials that can withstand large deformations and can be easily compressed without being mechanically damaged. Shape-defined macroporous alginate-based scaffolds prepared with different geometric sizes and shapes can be successfully passed through a surgical needle without mechanical fracture. However, after the shear force is removed, the scaffolds quickly recover their original shapes (Fig. 1 *C* and *D*).

Hydrogel Characterization. ^{1}H NMR was used to characterize vinyl conversion of MA-alginate macromonomer after polymerization. Full disappearance of methylene protons (δ5.3–5.8 ppm) was reached after cryopolymerization of MA-alginate macromonomer in the presence of the radical initiator system (Fig. S2). This suggests complete consumption of the reactive pendant methacrylate groups grafted to the alginate backbone.

A typical feature of cryogelation is the ability to produce a system of interconnected macropores, and the microstructure of alginate cryogels was evaluated by various microscopic observations. SEM demonstrated pore sizes in the range of 10–600 μm, with an average pore size between 150 and 200 μm (Fig. 2*A*). This contrasts with traditional nanoporous hydrogels that are produced from the same precursors, but at a temperature above freezing (Fig. 2*B*). X-ray micro-computed tomography (micro-CT) also demonstrated the highly macroporous and interconnected pore structure of cryogels (Fig. 2*C*), compared with traditional scaffolds (Fig. 2*D*), where pores were smaller, less interconnected, and poorly distributed. Reconstructed 3D images of alginate cryogels emphasized the highly porous interconnected and well-controlled internal microarchitecture (Fig. 2*E*). Finally, traditional nanoporous hydrogels are monophasic with a homogeneous distribution of cross-links throughout the construct, resulting in a transparent nanoporous gel (Fig. 2*F*). However, the phase separation that occurs during cryogelation leads to a heterogeneous opaque hydrogel consisting of macropores and tightly cross-linked pore walls. Treatment of nanoporous hydrogels with calcium ions led to additional cross-linking, as indicated by substantial shrinkage. In contrast, cryogels exhibited little volume change with calcium exposure, suggesting saturation in cross-linking following cryogelation.

Next, the effect of the network microstructure on the gel mechanical properties was assessed. Conventional gels give a Young's modulus of 42 ± 4 kPa in compression, whereas cryogels with identical polymer composition had a dramatic reduction in the modulus, to 4 ± 2 kPa, as expected. Examination of stress–strain curves revealed that the nanoporous gels could be strained by ∼16% before mechanical fracture (Fig. 3*B*). In comparison, cryogels exhibited much larger deformation under lower mechanical stress. Cryogels exhibited 90% or more compression strain without permanent deformation or mechanical destruction, demonstrating their potential as a biomaterial for minimally invasive delivery. The cryogels also displayed shape-memory properties as, once the mechanical load was removed, the elastically deformed gel immediately returned to its original, undeformed shape in less than a second (Movie S1). Highly interconnected pores (92% connectivity) were observed for the cryogels prepared at −20 °C, whereas poorly interconnected pores (4% connectivity) were observed in conventional hydrogels prepared at RT (Fig. 3*C*).

Conventional gels and the cryogels were also subjected to swelling measurements. Cryogels exhibited the highest swelling ratio (Q_M = 68 ± 5). In comparison, the conventional gels exhibited a lower swelling ratio (Q_M = 43 ± 3), presumably due to a lower water absorption capacity of nanoporous gels. As expected, Q_M decreases when the gels are exposed to Ca^{2+}, as further increases in the cross-link density of the gels will diminish swelling. The volumetric change with calcium exposure was less apparent in cryogels, confirming the limited capacity of the system to incorporate further cross-links within the highly condensed and cross-linked pore walls. Characterization of gels with constant geometry, but different dimensions, indicated that the gel size did not affect the physical properties of cryogels (Fig. S3) under the cryogelation conditions used in this study.

Injectability of Cryogels. The ability of cryogels to flow through a conventional-gauge needle, and then regain their original shapes once delivered was next examined. Subject to shear stress during injection, cryogels experience a body force proportional to the applied pressure, resulting in the collapse of the polymeric network. Square-shaped alginate cryogels were suspended in 0.2 mL of PBS and successfully syringe injected by means of a 16-gauge needle (Movies S2 and S3). The large volumetric change of the macroporous gels was presumably caused by a reversible collapse of the pores. After injection, deformed gels rapidly returned to their original, undeformed configuration (shape recovery, 92%; Fig. S4), as surrounding water was reabsorbed into the gels (Movie S4). To test whether cryogels could be delivered in the body, sterile square-shaped cryogels suspended in 0.2 mL of PBS were injected subcutaneously (s.c.) in the backs of C57BL/6J mice. After 2 d, the injected scaffolds were explanted for visual examination. The cryogels recovered their original shapes and remained localized at the point of introduction (Fig. S5). There was no perceptible inflammatory response outside the scaffold margin and no capsule formation at this time point.

Controlled Release of Biomolecules. We next examined the utility of cryogels for controlled delivery of biomolecules in vivo. BSA was suspended in a solution of gel precursors either as a free protein

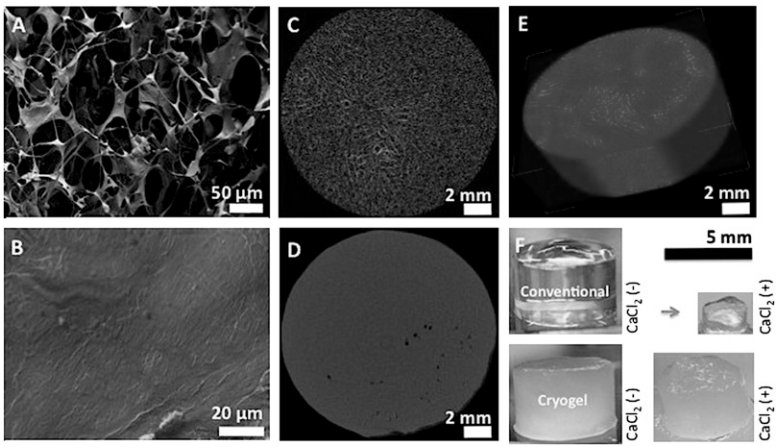

Fig. 2. SEM cross-sectional image of 1% (wt/vol) MA-alginate cryogel showing interconnected macroporous network (*A*) and nanoporous structure of conventional hydrogels (*B*). Two-dimensional micro-CT images of alginate cryogel (*C*) and conventional hydrogel (*D*), and reconstructed three-dimensional micro-CT image of alginate cryogel (*E*). Photographs of cylindrical MA-alginate hydrogels, demonstrating the effect of Ca^{2+} treatment on cryogels and conventional hydrogels (*F*).

[rhodamine-labeled BSA (Rhod-BSA)] or as a reactive substance [methacrylated rhodamine-labeled BSA (Rhod-BSA-MA)] before cryogenic treatment to allow their incorporation in the pore walls of the cryogel. This gives rise to a macroporous matrix immobilizing BSA (encapsulation efficiency: $E_E = 90\%$; Fig. S4). BSA-containing alginate cryogels were then syringe delivered into the s.c. space of C57BL/6J mice. Each mouse received a total of two cryogel injections, cross-linked Rhod-BSA-MA (right flank) and encapsulated Rhod-BSA (left flank). The dye-labeled cryogels could be readily located in tissue at the site of injection (Fig. 4*A*). At 3 d postinjection, one set of the square-shaped scaffolds located underneath the skin (Fig. 4*B*) was surgically removed and analyzed. The explanted cryogels demonstrate no alteration in size, and minimal inflammation was observed by histology (Fig. 4*C*). The scaffolds were encased within host tissue in vivo (Fig. 4*D*), and fluorescent microscopy revealed the original geometry of the gels, indicating that the structural integrity and the geometric square shape was retained within the s.c. pocket (Fig. 4*E*). Sustained release of BSA was achieved from the injected square-defined scaffolds as indicated by the spread of Rhod-BSA into the surrounding tissue over time (Fig. 4*E*), and diminishing fluorescence of the cryogels (Fig. 4*F*). The release profiles for physically entrapped and chemically anchored BSA were similar, suggesting that protein release may be triggered by matrix degradation rather than by diffusion. The delayed release profiles suggest a very slow degradation rate of the matrix.

The release of granulocyte–macrophage colony-stimulating factor (GM-CSF), an important hematopoietic growth factor and immune modulator, was also studied to examine the ability of the cryogels to provide a sustained release of potentially useful protein drugs. Approximately 80% of encapsulated GM-CSF was released from the cryogels within 3 d, and release was nearly complete over a period of 4 wk (Fig. S6).

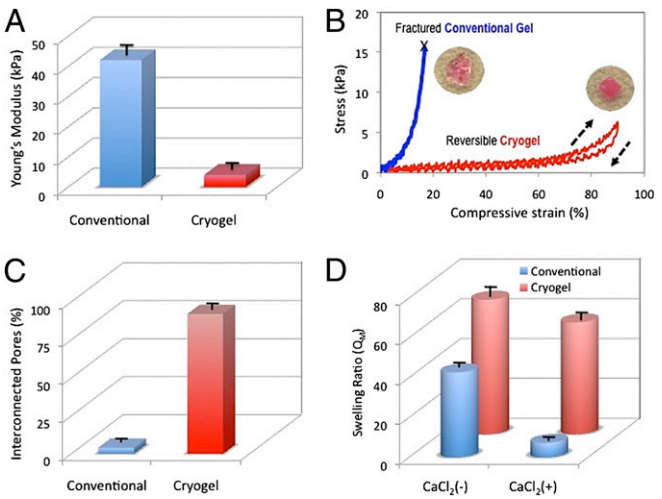

Fig. 3. Comparison of physical properties of conventional nanoporous gels versus cryogels. Both gel types were fabricated using 1% (wt/vol) MA-alginate. Young's moduli for alginate cryogels and conventional hydrogels (*A*). Stress vs. strain curves for macroporous and nanoporous rhodamine-labeled alginate hydrogels subjected to compression tests (*B*). Evaluation of pore connectivity (*C*) and weight swelling ratio (*D*) of macroporous and conventional alginate hydrogels. Swelling ratios were determined for gels in the absence (–) and presence (+) of $CaCl_2$. Values in *A*, *C*, and *D* represent mean and SD ($n = 4$).

Loading Cryogels with Cells for Transplantation. The ability of cryogels to be loaded with cells for transplantation was examined in the next series of studies. A cell-adhesive peptide, containing the RGD sequence, was coupled to alginate via covalent coupling of the peptide to polymerizable acryloyl-PEG-*N*-hydroxysuccinimide (ACRL-PEG-NHS) to promote cell adhesion. Cells were initially entrapped in cryogels (Fig. S7), resulting in cells being homogeneously distributed in gel pores. Adhesion of cells to the cryogel matrix occurs when the accessible RGD peptides immobilized on the matrix interact with integrin receptors on cell surfaces. RGD modification of alginate cryogels enhanced attachment (Fig. 5*A*) and spreading of cells (Fig. 5*B*), as contrasted to many fewer adherent cells in cryogels that were not modified with a peptide (Fig. 5*C*) or were modified with a non–cell-adhesive control peptide (Fig. 5*D*).

One important aspect of the alginate cryogel technology is its potential to be used as an injectable cell delivery vehicle. The effect of fluid velocity, pressure, and shear stress resulting from injection on cell retention and viability was also analyzed. Injection had a minimal effect on the release of bound cells (cell retention efficiency: $CR_E = 80\%$; Fig. S8), and the viability of cells in injected cryogels was $92 \pm 3\%$ (Fig. 5*E*), comparable with the control group. The proliferative capacity of cells was not lost, as the cells grew to confluency within the cryogels after incubation postinjection (Fig. 5*F*).

The ability of cryogels to transplant and subsequently localize cells was next examined. Square-shaped rhodamine-labeled RGD-containing alginate cryogels ($4 \times 4 \times 1$ mm) were prepared (Fig. 6*A*), purified, sterilized, and subsequently seeded with bioluminescent reporter cells, and maintained in culture for 1 d to promote cell adhesion (Fig. 6 *B* and *C*). Healthy C57BL/6J mice received a s.c. injection on their backs of a series of bioluminescent reporter cells seeded on rhodamine-labeled cryogels with and without adhesion peptide. As a control, a bolus of free cells was also injected. Immediately after injection, detection of red-emitting rhodamine dyes indicated successful injection and in vivo localization of fluorescently-labeled scaffolds (Fig. 6*D*). Both types of cryogels maintained cells at the point of introduction area after 2 d (Fig. 6*E*) as the bioluminescence was particularly bright, whereas simple cell injections did not. RGD appeared to lead to more cell retention. By day 15, RGD had a major effect in supporting cell

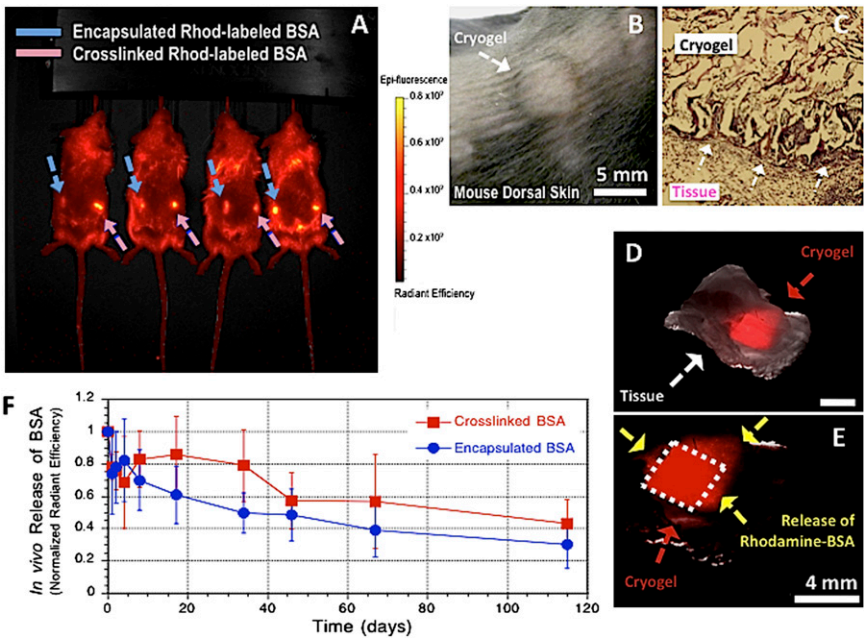

Fig. 4. Minimally invasive s.c. injection of alginate cryogels into the backs of C57BL/6J mice (*A*). Hydrogel localization after s.c. injection of preformed rhodamine-labeled 1% MA-alginate cryogels (4 × 4 × 1 mm) in the subcutis of a mouse after 3 d (*B*). Histological analysis (H&E stain) of explanted alginate cryogel at day 3. The arrows indicate the interface between the s.c. connective tissue (*Lower Left*) and the cryogel matrix (*Upper Right*). (Magnification: 10×.) (*C*). Photographs showing merged phase-contrast and fluorescence of s.c. injected rhodamine-labeled alginate macroporous scaffold with restoration of geometry after placement (*D*). Three days postinjection, the dashed lines indicate original square-shaped geometry of recovered scaffolds and the arrows show the spread of released BSA into the surrounding tissue (*E*). In vivo release profiles of cross-linked (chemically anchored) or encapsulated (physically entrapped) rhodamine-labeled BSA containing injected cryogels (*F*). Values represent mean and SD ($n = 4$).

engraftment, as many more transplanted cells were present compared with cryogels without RGD peptides (Fig. 6*F*).

Discussion

The results of this study suggest that a minimally invasive delivery approach can be used to introduce preformed shape-memory macroporous cryogels via needle–syringe injection into the body without mechanical fracture. These cryogels could be readily injected into the s.c. layer of the skin, used to fill in vivo tissue defects and cavities, or used as patches on internal organs. These materials have an interconnected macroporous architecture, which is advantageous with respect to their ability to facilitate cellular infiltration, and incorporation of payloads (e.g., cells) after devices are manufactured. The most important requirement of these materials for minimally invasive therapies is the ability to collapse, and faithfully and rapidly resume their original structure once placed in the body. Shape memory allows for this function. Furthermore, the ability of these materials to reassume specific, predefined shapes after injection is likely to be useful in applications such as tissue patches (e.g., cardiac patches) where one desires a patch of a specific size and shape, or when one desires to fill a large defect site with multiple smaller objects that pack in such a manner to leave voids that enhance diffusional transport to/from the objects and the host, and promote vascularization around each object (30, 31). The polymeric system can be used as a delivery device for biomolecules, including proteins, as long-term sustained release of encapsulated rhodamine-labeled BSA and GM-CSF demonstrate. Also, the feasibility of this approach to transplant cells was examined with bioluminescent reporter cells. The bioactive cryogels provided a favorable microenvironment to facilitate cell survival and engraftment of transplanted cells.

Cryogels have tissue-like compliance and are mechanically robust due to a highly cross-linked polymer phase that results from sterically entangled polymer chains, a high degree of chemical modification of alginate, a high polymer concentration, and nearly complete reactivity of methacryoyl groups during cryogelation. Unlike conventional gels, a unique characteristic of these scaffolds is that when an appropriate shear stress is applied, the cryogels can be reversibly compressed at over 90% strain levels, resulting in injectable macroporous preformed scaffolds. The large volumetric change of the cryogels is caused by reversible collapse of the interconnected pores forcing water contained in the macropores to flow out of the gel. The cryogels have the ability to memorize a macroscopic and permanent shape, to be manipulated and temporarily collapsed, and then later to be relaxed to their original structure without residual permanent deformation. The relaxation is associated with the energy stored during the elastic gel collapse. The gels in this study were fabricated with high–molecular-weight alginate but can be formed with a variety of materials, including biodegradable polymers. One could further tune their performance by altering their composition, formulation, and degradation profiles. The ability of these gels to be syringe

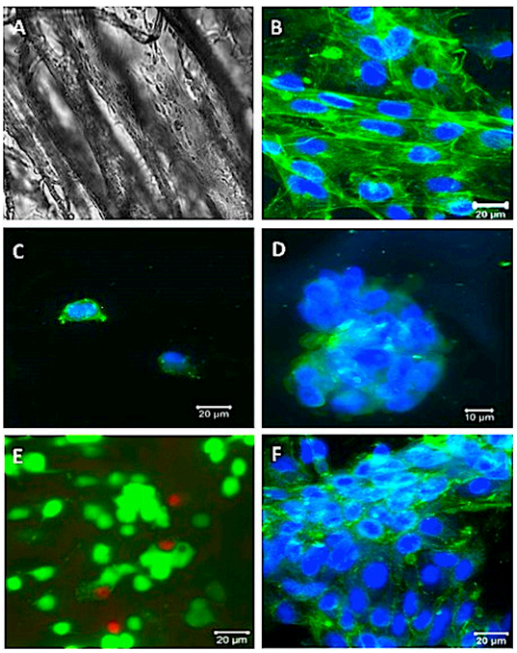

Fig. 5. Adhesion of MSC cells in MA-alginate cryogels. Phase-contrast image showing elongated cells in RGD-containing cryogels (*A*). Confocal micrographs of seeded cells after 5 d of culture are shown in a typical RGD-modified cryogel (*B*), unmodified cryogel (*C*), and RGE-modified cryogel (*D*). Live/dead cell assay of MSCs (*E*) (1 d incubation postinjection) and confocal image showing cells (*F*) (6 d incubation postinjection) in RGD-modified MA-alginate cryogels. Cryogels were injected through a 16-gauge needle before imaging (*E* and *F*). (Scale bars: *A*–*C*, *E*, *F*, 20 μm; *D*, 10 μm.)

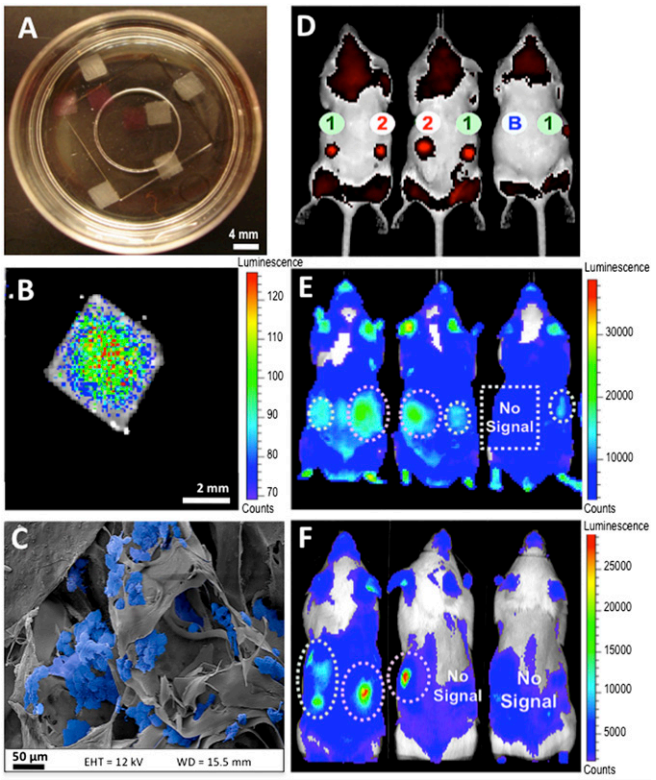

Fig. 6. Injectable preseeded scaffolds promote in situ localization and retention of bioluminescent reporter cells. Photographs showing alginate cryogel scaffolds (white) and rhodamine-labeled alginate scaffolds (pink) (*A*). Bioluminescent cells were seeded on 1% RGD-modified MA-alginate cryogels at a concentration of 200×10^3 cells/scaffold, and cultured for 1 d. Optical imaging depicts distribution of bioluminescent cells (*B*). SEM image shows cells (pseudocolored blue) homogeneously adherent to the gel (*C*). Real-time fluorescence in vivo imaging showing injected Rhod-labeled cryogels. Cells injected s.c. via Rhod-labeled cryogels (1), Rhod-labeled RGD-cryogels (2), or as a free-floating cell suspension (*B*) in BALB/c mice at day 0 (*D*). Noninvasive bioluminescence in vivo imaging of transplanted cells in BALB/c mice at day 2 (*E*) and day 15 (*F*) postinjection. The same mice were used in each of these images and were arranged in the same relative positions before imaging (*D–F*).

delivered at a specific location without the need of an invasive surgery may decrease scarring, lessen the risk of infection, and reduce recovery times compared with traditional procedures. The maximum injectable gel size investigated to date is $8 \times 8 \times 1$ mm for the square-shaped cryogels. However, the technique used to fabricate gels is amenable to scaling up for larger injectable structures.

These cryogels can act as a delivery vehicle for therapeutics and cells, with sustained release over time. By providing a protein drug depot at the site of injection, the cryogels can potentially achieve high local protein concentrations without systemic exposure to the bioactive proteins. Biomacromolecules, such as BSA used here as a model protein and GM-CSF, can be physically entrapped during polymerization. Due to the large size of the protein paired with a dense polymer microstructure, these proteins were retained in the cryogel during injection and released in vitro and in vivo in a sustained fashion.

The open pore structure of the cryogels with bioactive surfaces and tissue-like elasticity provide an appropriate microenvironment for cells. Absorption of a cell suspension occurs through the pores by convection, which was used to uniformly seed cells throughout the gel. Cell entrapment results in a very efficient immobilization system, in which the cells are initially caged in gel pores. To prevent anoikis and to retain cells, adhesion peptides were grafted to the cryogels (32). During the syringe injection of cell-seeded cryogels, over 80% of cells initially in cryogels were retained, with high viability. These cell-seeded injectable porous scaffolds are potentially of wide utility for tissue regeneration; one could apply this technology to develop biologically active scaffolds that controllably deliver growth factors while providing cellular building blocks to enhance tissue formation. In an attempt to improve cell transplantation, biocompatible macroporous alginate cryogels have been used to create a niche that provides the appropriate microenvironment to promote survival of transplanted cells. This microenvironment includes chemical and physical cues designed to guide cell growth and integration with the host tissue. The uniform distribution and viability of seeded cells are unaffected by the shear thinning during injection and the gel constructs remain at the point of introduction, suggesting that the localized delivery of gels may be useful for the delivery of cells in close proximity to a lesion site in tissue regeneration efforts. More broadly, this may provide a core technology useful to solve some of the fundamental problems associated with current cell-based therapies—the rapid loss of cell viability, low engraftment efficiency, and absence of control over cell fate after introduction into the body (32). The independent tuning of cell-adhesive properties is desirable in creating a cellular microenvironment suitable for survival, consistent with previous studies (33). Biomimetic cryogels seeded with bioluminescent reporter cells and introduced s.c. in mice showed enhanced bioluminescence signals, indicating that cell delivery using cryogels decreases cell loss from the injection site, enhances survival, and promotes engraftment of cells in vivo.

Materials and Methods

Materials. Sodium alginate with high guluronate content (LF 20/60) was purchased from ProNova Biomedical; and 2-morpholinoethanesulfonic acid (Mes), sodium chloride (NaCl), calcium chloride ($CaCl_2$) sodium hydroxide (NaOH), *N*-hydroxysuccinimide (NHS), 1-ethyl-3-(3-dimethylaminopropyl)-carbodiimide hydrochloride (EDC), AEMA, methacrylic anhydride (MAH), BSA, 5(6)-carboxy-X-rhodamine *N*-succinimidyl ester (rhodamine-NHS), MA, and acetone were purchased from Sigma-Aldrich. ACRL-PEG-NHS (3.5 kDa) was purchased from JenKen Technology. The integrin binding peptide $(Gly)_4$-Arg-Gly-Asp-Ala-Ser-Ser-Lys-Tyr was purchased from Commonwealth Biotech. Clonally derived murine mesenchymal stem cells (D1 MSCs) (ATCC) and luciferase-transduced B16-F10 cells (ATCC) were cultured in Dulbecco's modified Eagle medium (DMEM) supplemented with 10% (vol/vol) FBS and 1% (vol/vol) penicillin–streptomycin, all obtained from Invitrogen. Live/Dead Viability/Cytotoxicity Kit was purchased from Invitrogen. D-Luciferin was obtained from Gold Biotechnology.

Chemical Modification. MA-alginate was prepared by reacting alginate with AEMA. Sodium alginate (1 g) was dissolved in a buffer solution [0.6% (wt/vol), pH ~6.5] of 100 mM Mes. NHS (1.3 g) and EDC (2.8 g) were added to the mixture to activate the carboxylic acid groups of alginate. After 5 min, AEMA (2.24 g; molar ratio of NHS:EDC:AEMA = 1:1.3:1.1) was added to the product and the solution was stirred at RT for 24 h. The mixture was precipitated in acetone, filtered, and dried in a vacuum oven overnight at RT. ^{1}H NMR was used to characterize chemical modification of alginate and degree of functionalization of MA-alginate. Rhod-BSA-MA was prepared by reacting Rhod-BSA with MAH. Rhod-BSA was synthesized according to ref. 34. Rhod-BSA (100 mg) was dissolved in deionized water, and MAH (30 mg) was added to the mixture. After 30 min, the mixture was precipitated in an excess of acetone, filtered, and dried in a vacuum oven overnight at RT.

Hydrogel Fabrication. Macroporous and conventional (nanoporous) matrices were synthesized by redox-induced free-radical polymerization of MA-alginate in water. ACRL-PEG-G_4RGDASSKY and ACRL-PEG-G_4RGEASSKY were synthesized according to ref. 5. Alginate cryogels were synthesized by mixing 10 mg [1% (wt/vol)] of MA-alginate macromonomer in deionized water with tetramethylethylenediamine (TEMED) [0.5% (wt/vol)] and ammonium persulfate (APS) [0.25% (wt/vol)]. Fabrication conditions were chosen to allow the solution to freeze before the gelation takes place and thus eliminate much of the dependence of the resulting structure on freezing rate, object size, and geometry. More specifically, a very small amount of initiator was used, the precursor solution was precooled to 4 °C to decrease the rate of polymerization before freezing, and once the initiator was added to the prepolymer solution, the solution was quickly poured into a precooled (–20 °C) Teflon mold. The solution froze within a minute while a witness solution stored at 4 °C remained unpolymerized for at least 20 min. After a complete incubation period of 17 h, the gels were heated to RT to remove ice crystals and washed with deionized water.

Cell-adhesive cryogels were synthesized using ACRL-PEG-G_4RGDASSKY as a co-monomer [0.8% (wt/vol)] during the polymerization. Conventional hydrogels were cross-linked for 30 min at RT for a homogeneous gelation.

Polymer and Hydrogel Characterization. High-resolution ^{1}H NMR spectra were obtained in deuterium oxide (D_2O) using a Varian Unity-300 (300 MHz) NMR spectrometer (Varian). To analyze the methacrylation efficiency, ^{1}H NMR spectra were recorded for methacrylated alginate. ^{1}H NMR spectroscopy was also used to characterize vinyl group conversion after cryopolymerization. Details regarding the structural analysis of the macroporous gels, evaluation of pore connectivity, mechanics, and swelling ratio can be found in *SI Materials and Methods*.

Minimally Invasive Delivery of Scaffolds. Female C57BL/6J mice (n = 3; The Jackson Laboratory), 4–6 wk of age, were anesthetized with 2.5% isoflurane using an inhalation anesthesia system (E-Z Anesthesia; Euthanex). Each mouse received a s.c. dorsal injection of rhodamine-labeled cryogels suspended in 0.2 mL of PBS by means of a 16-gauge needle under the dorsal panniculus carnosus. Subsequently, mice were sacrificed, and the implants with the surrounding tissues were imaged using a Zeiss SteREO Lumar V12 stereomicroscope (Carl Zeiss) in both bright field and fluorescence. Specimens were also embedded in paraffin and 5-μm sections were stained with hematoxylin and eosin (H&E) for histological analysis. Animal work was performed under a protocol approved by the Harvard Standing Committee on Animals in compliance with the National Institutes of Health guidelines.

Controlled Release of Proteins. For the in vivo release study, rhodamine-labeled cryogels (physically entrapped or covalently anchored BSA) were s.c. injected in BALB/cJ mice (n = 5) by means of a 16-gauge needle under the dorsal panniculus carnosus. Release of fluorescent BSA was monitored over time using fluorescence images of mice on a Xenogen IVIS Spectrum system (Caliper Life Sciences). Per the manufacturer, regions of interest (ROIs) of equal areas were selected for all of the images centering upon the foci of greatest intensity ensuring both conditions had equivalent areas. The same boundary around the scaffold was used throughout the study to discriminate released BSA from retained BSA within the construct. Additional information for loading and release of GM-CSF from cryogels is available in *SI Text* (Fig. S6). Details regarding the preparation of BSA-containing cryogels can be found in *SI Materials and Methods*.

Cell Culture and Seeding of Cryogels. Before seeding cells, the cryogels were treated with 70% ethanol and washed with PBS. The cryogels were mechanically compressed to partially remove pore water under sterile conditions before cell seeding. Briefly, cells (D1 MSCs or B16-F10) were suspended in complete culture medium (DMEM supplemented with 10% FBS and 1% penicillin–streptomycin). Twenty microliters of cell suspension (10^6–10^7 cells/mL) were added in a dropwise manner on top of each square-shaped cryogel and incubated for 1 h. The cell-loaded cryogels were then cultured in FBS-supplemented media for the extent of the experiment (37 °C in 5% CO_2 environment). Cell distribution was noted to be homogeneous throughout the scaffold thickness.

Cell Viability Test. A live/dead assay was performed to evaluate cell viability in the cryogels. Briefly, the cell-laden cryogels in triplicate were incubated with the live/dead assay dye solution (Molecular Probes) containing 0.5 μL of calcein-AM and 2 μL of ethidium homodimer-1 in 1 mL of PBS. After 30-min incubation, the cryogels were rinsed with PBS and cells were imaged by confocal microscopy (Zeiss LSM 510). High-resolution image stacks were collected with 300-nm separation between slices (z-stacks). For each of the cryogels, four representative sections were imaged. Cell viability was calculated as the ratio of green fluorescence (live cell) surface area to the combined surface area of green fluorescence (live cells) and red fluorescence (dead cells).

Delivery of Cells. Localized delivery of cells was achieved by injecting cell-loaded cryogels directly into the area of interest. Cryogels were seeded with luciferase-transduced B16-F10 cells (~0.2×10^6 cells/cryogel) and incubated at 37 °C in 5% CO_2 for 1 d to allow cell adhesion. Female BALB/c mice (n = 3; The Jackson Laboratory), 4–6 wk of age, were anesthetized with 2.5% isoflurane using an inhalation anesthesia system. Each mouse received two s.c. dorsal injections by means of a 16-gauge needle under the dorsal panniculus carnosus, whereas one mouse was injected with free cells as a control. To create a space for gel recovery after injection, 200 μL of PBS was injected along with the cryogel to rehydrate the shape-memorizing cell delivery biomaterial and return it to its original size and shape in vivo. Optical bioluminescence images of mice were obtained using an IVIS live animal imaging system (Caliper Life Sciences). After intraperitoneal injection of the reporter probe D-luciferin (375 mg/kg body weight), mice were placed in the imaging chamber. High-sensitivity bioluminescent imaging was quantified by creation of polygonal regions of interest (ROIs).

ACKNOWLEDGMENTS. We thank J. A. Goss for his technical support. This work was supported by the Wyss Institute for Biologically Inspired Engineering at Harvard University, National Institutes of Health Grant 5R01DE019917-03, and Juvenile Diabetes Research Foundation Grant 5-2011-434.

1. Dellatore SM, Garcia AS, Miller WM (2008) Mimicking stem cell niches to increase stem cell expansion. *Curr Opin Biotechnol* 19(5):534–540.
2. Hubbell JA (1995) Biomaterials in tissue engineering. *Biotechnology (N Y)* 13(6):565–576.
3. Burdick JA, Prestwich GD (2011) Hyaluronic acid hydrogels for biomedical applications. *Adv Mater* 23(12):H41–H56.
4. Kretlow JD, Klouda L, Mikos AG (2007) Injectable matrices and scaffolds for drug delivery in tissue engineering. *Adv Drug Deliv Rev* 59(4–5):263–273.
5. Bencherif SA, et al. (2008) Influence of the degree of methacrylation on hyaluronic acid hydrogels properties. *Biomaterials* 29(12):1739–1749.
6. Bencherif SA, et al. (2009) End-group effects on the properties of PEG-co-PGA hydrogels. *Acta Biomater* 5(6):1872–1883.
7. Kim BS, Mooney DJ (1998) Development of biocompatible synthetic extracellular matrices for tissue engineering. *Trends Biotechnol* 16(5):224–230.
8. Mooney DJ, Baldwin DF, Suh NP, Vacanti JP, Langer R (1996) Novel approach to fabricate porous sponges of poly(D,L-lactic-co-glycolic acid) without the use of organic solvents. *Biomaterials* 17(14):1417–1422.
9. Mikos AG, et al. (1993) Preparation of poly(glycolic acid) bonded fiber structures for cell attachment and transplantation. *J Biomed Mater Res* 27(2):183–189.
10. Bennett DJ, Burford RP, Davis TP, Tilley HJ (1995) Synthesis of porous hydrogel structures by polymerizing the continuous phase of a microemulsion. *Polym Int* 36(3):219–226.
11. Nam YS, Park TG (1999) Biodegradable polymeric microcellular foams by modified thermally induced phase separation method. *Biomaterials* 20(19):1783–1790.
12. O'Brien FJ, Harley BA, Yannas IV, Gibson LJ (2005) The effect of pore size on cell adhesion in collagen-GAG scaffolds. *Biomaterials* 26(4):433–441.
13. Mikos AG, et al. (1994) Preparation and characterization of poly(L-lactic acid) foams for cell transplantation. *Polymer (Guildf)* 35(5):1068–1077.
14. Mikos AG, Sarakinos G, Leite SM, Vacanti JP, Langer R (1993) Laminated three-dimensional biodegradable foams for use in tissue engineering. *Biomaterials* 14(5):323–330.
15. Thornton AJ, Alsberg E, Hill EE, Mooney DJ (2004) Shape retaining injectable hydrogels for minimally invasive bulking. *J Urol* 172(2):763–768.
16. Plieva FM, Galaev IY, Noppe W, Mattiasson B (2008) Cryogel applications in microbiology. *Trends Microbiol* 16(11):543–551.
17. Lozinsky VI, et al. (2003) Polymeric cryogels as promising materials of biotechnological interest. *Trends Biotechnol* 21(10):445–451.
18. Hwang Y, Zhang C, Varghese S (2010) Poly(ethylene glycol) cryogels as potential cell scaffolds: Effect of polymerization conditions on cryogel microstructure and properties. *J Mater Chem* 20(2):345–351.
19. Kathuria N, Tripathi A, Kar KK, Kumar A (2009) Synthesis and characterization of elastic and macroporous chitosan-gelatin cryogels for tissue engineering. *Acta Biomater* 5(1):406–418.
20. Bölgen N, et al. (2009) Tissue responses to novel tissue engineering biodegradable cryogel scaffolds: An animal model. *J Biomed Mater Res A* 91(1):60–68.
21. Bölgen N, et al. (2008) Three-dimensional ingrowth of bone cells within biodegradable cryogel scaffolds in bioreactors at different regimes. *Tissue Eng Part A* 14(10):1743–1750.
22. Christman KL, et al. (2004) Injectable fibrin scaffold improves cell transplant survival, reduces infarct expansion, and induces neovasculature formation in ischemic myocardium. *J Am Coll Cardiol* 44(3):654–660.
23. Yao J, Tao SL, Young MJ (2011) Synthetic polymer scaffolds for stem cell transplantation in retinal tissue engineering. *Polymers* 3(2):899–914.
24. Yu L, Ding J (2008) Injectable hydrogels as unique biomedical materials. *Chem Soc Rev* 37(8):1473–1481.
25. Jeong B, Kim SW, Bae YH (2002) Thermosensitive sol-gel reversible hydrogels. *Adv Drug Deliv Rev* 54(1):37–51.
26. Ruel-Gariépy E, Leroux JC (2004) In situ-forming hydrogels—review of temperature-sensitive systems. *Eur J Pharm Biopharm* 58(2):409–426.
27. Guvendiren M, Lu HD, Burdick JA (2012) Shear-thinning hydrogels for biomedical applications. *Soft Matter* 8(2):260–272.
28. Silva EA, Mooney DJ (2007) Spatiotemporal control of vascular endothelial growth factor delivery from injectable hydrogels enhances angiogenesis. *J Thromb Haemost* 5(3):590–598.
29. Augst AD, Kong HJ, Mooney DJ (2006) Alginate hydrogels as biomaterials. *Macromol Biosci* 6(8):623–633.
30. Leor J, Amsalem Y, Cohen S (2005) Cells, scaffolds, and molecules for myocardial tissue engineering. *Pharmacol Ther* 105(2):151–163.
31. Halberstadt C, et al. (2002) A hydrogel material for plastic and reconstructive applications injected into the subcutaneous space of a sheep. *Tissue Eng* 8(2):309–319.
32. Cooke MJ, Vulic K, Shoichet MS (2010) Design of biomaterials to enhance stem cell survival when transplanted into the damaged central nervous system. *Soft Matter* 6(20):4988–4998.
33. Straley KS, Heilshorn SC (2009) Independent tuning of multiple biomaterial properties using protein engineering. *Soft Matter* 5(1):114–124.
34. Huebsch N, et al. (2010) Harnessing traction-mediated manipulation of the cell/matrix interface to control stem-cell fate. *Nat Mater* 9(6):518–526.